Published in final edited form as:
Eur J Neurosci. 2011 November ; 34(9): 1419–1431. doi:10.1111/j.1460-9568.2011.07861.x.

Carbonic anhydrase-related protein VIII is expressed in rod bipolar cells and alters signaling at the rod bipolar to AII-amacrine cell synapse in the mammalian retina

T. Puthussery, **J. Gayet-Primo**, and **W. R. Taylor**
Department of Ophthalmology, Casey Eye Institute, Oregon Health and Sciences University, Portland, OR, USA

Abstract

Mutation of the gene encoding carbonic anhydrase-related protein VIII (CAVIII) results in motor coordination deficits in mice and humans, due to loss of this protein in Purkinje cells of the cerebellum. Recent studies have indicated that the CAVIII gene, *Car8*, is also expressed in rod bipolar cells (RBCs), a critical glutamatergic neuron for scotopic vision. We investigated the localization of CAVIII in the mouse and macaque retina, and utilized the *wdl* mouse, which has a null mutation in the *Car8* gene, to determine how the loss of CAVIII affects retinal signaling. CAVIII immunoreactivity was observed in RBCs, with particularly high staining intensity in the axon terminals. In addition, weaker staining was observed in a subset of cone bipolar cells and γ-aminobutyric acid (GABA)ergic amacrine cells. Light-evoked current and voltage responses of RBCs were not altered in the *wdl* mutant. However, light-evoked current responses from the AII-amacrine cell, a postsynaptic partner at the RBC ribbon synapse, were significantly larger, and more prolonged than in control mice. These changes could not be attributed to alterations in calcium current activation or inactivation, or to changes in the density of RBCs. Furthermore, no gross synaptic alterations were evident in the *wdl* mutant at the light or ultrastructural level. These data provide evidence that the CAVIII protein, which is highly conserved in vertebrates, is selectively expressed within neural circuits, and may be important for modulating retinal neurotransmission.

Keywords

amacrine cell; Car8; synaptic transmission; waddles mouse

Introduction

The *Car8* gene encodes carbonic anhydrase-related protein VIII (CAVIII), which is one of 16 carbonic anhydrase (CA) isoforms found in mammalian species. The majority of CA isoforms catalyse the reversible hydration of carbon dioxide; however, CAVIII is one of three isoforms that is catalytically silent due to the absence of zinc coordinating histidine residues at the active site (Kato, 1990; Sjoblom *et al.*, 1996). The role of the acatalytic isoforms is unknown; however, the high degree of conservation of the DNA and protein sequences suggests an important biological function (Skaggs *et al.*, 1993).

In the brain, CAVIII is abundantly expressed in cerebellar Purkinje neurons (Kato, 1990; Jiao *et al.*, 2005), and has also been localized to hippocampus, medial habenulae, thalamus

Correspondence: Dr T. Puthussery, as above. puthusse@ohsu.edu.

and cerebral cortex (Lakkis *et al.*, 1997). The *waddles* (*wdl*) mouse, which has a spontaneous null mutation of *Car8*, exhibits gait ataxia and dystonia (Jiao *et al.*, 2005). Similarly, human patients with mutations in *CA8* exhibit ataxia, mild mental retardation and a predisposition to quadrupedal gait (Turkmen *et al.*, 2009). The *wdl* mouse has no gross morphological abnormalities in the cerebellum; however, alterations have been documented at the ultrastructural level at synapses between Purkinje cell dendritic spines and parallel fiber varicosities, suggesting a role for CAVIII in synaptic formation and/or maintenance (Hirasawa *et al.*, 2007). The same study demonstrated a reduction in the frequency of spontaneous miniature excitatory postsynaptic currents (EPSCs) in Purkinje cells. CAVIII has been reported to interact with the IP3 receptor type 1 (IP3R1), and reduce the affinity of these receptors for the ligand, IP3 (Hirota *et al.*, 2003), which could produce alterations in intracellular calcium dynamics.

Expression studies have demonstrated the presence of *Car8* in the eye (Aspatwar *et al.*, 2010), and enrichment of *Car8* in a subset of retinal neurons, the rod bipolar cells (RBCs; Kim *et al.*, 2008); however, no evidence for protein expression has been described. The RBCs are a critical element in the scotopic signaling pathway in the retina, which mediates vision at absolute threshold. The circuitry of this pathway has been well characterized (for review, see Dacheux & Raviola, 1986), and thus provides an excellent system to further investigate the function of this protein. Here, we describe the localization of CAVIII in the mouse and primate retina, and show that loss of CAVIII alters signaling at the rod bipolar to AII-amacrine cell (AII-AC) synapse.

Materials and methods

Animals and tissue preparation

The waddles (wdl; C57BLKS/J-Car8^{wdl}/J; Jackson Laboratories) mouse has a spontaneously occurring 19-nucleotide deletion in exon 8 of the *Car8* gene that results in complete absence of CAVIII protein (Jiao *et al.*, 2005). By 2 weeks old, the homozygous mutants (*wdl*/*wdl*) display a wobbly side-to-side gait that persists into adulthood. Heterozygote animals (*wdl*/+) have no phenotype. A breeding colony was established by crossing homozygote mice with heterozygote mice obtained from the Jackson Laboratory. The animals were maintained on a 12-h light/12-h dark cycle. Adult mice (2–6 months) were used for all experiments. Homozygous mice were identified by their abnormal gait and littermate heterozygotes were used as controls. C57BL6 mice were also used for immunohisto-chemical experiments. Prior to experimentation, adult mice were anesthetized by intraperitoneal injection of sodium pentobarbital (0.1 mL, 100 mg/mL) and then killed by cervical dislocation. Mice used for electrophysiological recordings of light-evoked responses were dark-adapted for a period of at least 10 h prior to experimentation. Adult Sprague–Dawley rats were killed with carbon dioxide. Retinae from a female rhesus macaque, aged ~15 years, were collected under the tissue distribution program from the Oregon National Primate Research Center. All animal procedures were in accordance with the National Institutes of Health guidelines, and were approved by the Oregon Health and Science University Institutional Animal Care and Use Committee.

Indirect immunofluorescence immunohistochemistry

For immunohistochemistry, the eyes were enucleated, the anterior segment and vitreous was removed, and the posterior eyecups were immersion fixed for 30–60 min in 4% paraformaldehyde in 0.1 M phosphate buffer at 25 °C (pH 7.4). For vertical sections, the tissue was cryoprotected in graded sucrose solutions (10, 20, 30%), and sectioned at 14 μm. Non-specific binding sites were blocked with an incubation buffer (IB) containing 3% normal horse serum, 0.3% Triton X-100 (Tx-100) and 0.025% NaN_3 in 0.1 M phosphate-

buffered saline (PBS; pH 7.4) for 10 min. Primary antibodies were diluted in IB and applied to tissues for 2 h at 25 °C. Secondary antibodies were diluted 1: 800 in IB (without Tx-100) and applied to sections for 1 h at 25 °C. For immunohistochemistry on retinal whole-mounts, the concentration of Tx-100 in the IB was increased to 1%, primary antibodies were applied for 7–10 days at 25 °C, and secondary antibodies were applied overnight at 25 °C. Secondary antibodies were conjugated to Alexa Fluor 488, 594 or 647 (Invitrogen, Carlsbad, CA, USA), and were raised in donkey, with the exception of the anti-guinea pig secondary antibodies, which were raised in goat. For double- or triple-labeling experiments, sections were incubated in a mixture of primary antibodies followed by a mixture of secondary antibodies. Details of the primary antibodies used in this study are shown in Table 1.

Cell counts

RBCs were counted in whole-mount mouse retinas immunostained with protein kinase C (PKC)-α. For each genotype, seven fields of 0.019 mm^2 were imaged from within 2 mm of the optic nerve, and the number of PKC-α-immunopositive axons was counted using the 'Cell Counter' tool in IMAGE J.

Western blotting

Retinal and cerebellar tissue was placed in lysis buffer containing PBS (pH 7.2) supplemented with 150 mM NaCl, 5 mM EDTA, 0.05% Tx-100, and a protease and phosphatase inhibitor cocktail (Thermo Sci, Rockford, IL, USA). The tissue was briefly sonicated, then incubated on ice for 60 min. Cell debris was removed by centrifugation at ~13 000 ***g*** for 10 min, and the total protein concentration of the supernatant was determined using the BCA assay (Pierce). Samples were mixed with a sodium dodecyl sulfate (SDS) sample buffer (Thermo Sci #39001 + 6.25% β-ME), and separated on precast 4–20% gels (Precise, Pierce). Proteins were transferred onto nitrocellulose membranes and subjected to Western blot analysis using an anti-rabbit Alexa Fluor 680-conjugated secondary antibody and the Odyssey infrared imaging system (LI-COR Biosciences).

Electron microscopy

Posterior eyecups were placed in a fixative containing 2% paraformaldehyde, 2% glutaraldehyde, 3% sucrose and 1 mM calcium chloride in 0.1 M cacodylate buffer (pH 7.4) for 2 h at 25 °C. Eyecups were treated for 1 h in 2% osmium tetroxide, dehydrated through graded ethanol solutions and embedded in Embed 812 resin. Sections were cut at 70 nm, contrasted with lead citrate and uranyl acetate, and viewed on a Tecnai TM12 electron microscope at an operating voltage of 80 kV. Images were acquired on a Gatan digital camera.

Microscopy and imaging

Confocal micrographs were acquired on an Olympus Fluoview 1000 confocal microscope with a 40 × (1.3 N.A.) or 60 × (1.42 N.A.) oil-immersion objective. Images shown herein are from a single image plane or from projected image stacks where indicated. Further processing of confocal and electron micrographs was limited to adjustment of the brightness, contrast and sharpness of images with Adobe Photoshop CS. Any such modifications were applied uniformly across the entire image.

Electrophysiology

Vertical slices of mouse retina were prepared using methods described previously (Puthussery *et al.*, 2009). For recordings of light-evoked responses, cells were visualized and targeted under infrared illumination; however, the preparation was periodically exposed to dim red illumination from an LED (620 nm peak emission) when electrodes were replaced.

For calcium current recordings, light-adapted slices were used. In both cases, the retina was isolated from the posterior eyecup, mounted ganglion cell side down on a 0.8-μm cellulose membrane filter (Millipore, Bedford, MA, USA), and vertically sliced (~300 μm) using a Vibratome 600 tissue chopper. Slices were transferred to the recording chamber and perfused at a rate of ~2 mL/min with bicarbonate-buffered Ames medium (US Biologicals, Swampscott, MA, USA) continuously bubbled with 95% O_2, 5% CO_2. For recording of calcium currents, inhibitory inputs were blocked by inclusion of 10 μM SR 95531, 30 μM TPMPA and 1 μM strychnine to the bath solution. All recordings were performed at 32–33 °C. Slices were viewed with an Olympus BX51 upright microscope fitted with a 40 ×/0.8 water immersion objective and infrared gradient contrast optics (Dodt *et al.*, 2002). RBCs and AII-ACs were identified by their characteristic morphology and light responses.

Patch electrodes were fabricated from thick-walled borosilicate glass to have a resistance of 10–15 MΩ. For recordings of RBC and AII-AC light-evoked responses, the electrodes contained an intracellular solution comprising (in mM): K-methylsulfonate, 135; KCl, 6; Na_2-ATP, 2; Na-GTP, 1; EGTA, 1; $MgCl_2$, 2; Na-HEPES, 5; and adjusted to pH 7.35 with KOH. For recordings of voltage-gated calcium currents and AII-AC light-evoked current–voltage (I–V) relations, the internal solution contained (in mM): Cs-gluconate, 135; CsCl, 6; Na_2-ATP, 2; Na-GTP, 1; EGTA, 1; $MgCl_2$, 2; Na-HEPES, 5; and adjusted to pH 7.35 with CsOH. Alexa 488 or 594 hydrazide (50–100 μM) was added to these solutions for morphological identification of recorded cells.

Whole-cell voltage-clamp and current-clamp recordings were made with a HEKA EPC-10 patch-clamp amplifier. To minimize possible contamination of the light-evoked currents with γ-aminobutyric acid (GABA)ergic or glycinergic amacrine cell feedback, we set the holding potential to −70 mV, close to the predicted chloride equilibrium potential. All reported holding potentials were corrected for the liquid junction potential, which was calculated to be ~10 mV. Due to rapid rundown of light-evoked currents in RBCs, only recordings obtained within 1 min of break-in were used for subsequent analysis. Series resistance averaged 21.4 ± 1.9 MΩ (n = 21, ± SEM), and was compensated for by ~60–70% during the recordings of the calcium currents. Series resistance compensation was not applied during recordings of light-evoked currents but, due to the relatively small amplitudes of the EPSCs, the voltage error is estimated to be < 5% at −70 mV. The linear excitatory and inhibitory synaptic conductances shown in Fig. 8 were estimated from the current response (Fig. 8A), as described previously (Venkataramani *et al.*, 2010). For current-clamp recordings, hyperpolarizing current was injected to bring the cells close to a potential of approximately −70 mV. Responses were digitally sampled at 5 kHz and filtered at 2 kHz. Current and voltage traces were further filtered off-line with a −3-dB corner frequency of 100 Hz. Off-line filtering and analysis was performed using custom analysis routines in IGOR PRO (Wavemetrics, Lake Oswego, OR, USA). Light responses were elicited by diffuse illumination at a peak wavelength of 525 nm, using a LED projected through the microscope eyepiece and focused onto the preparation. Flash intensity was varied by altering the duration of the flash from 0.01 to 20 ms, which is within the integration time of mouse rod photoreceptors (~200 ms; Burns *et al.*, 2002). Light intensity was calibrated using a UDT photometer (UDT Instruments, San Diego, CA, USA) and converted to photons/μm^2.

Statistical analysis

The intensity–response families from heterozygous mice were compared with that of *wdl* mutant mice using a two-way analysis of variance (ANOVA) test (intensity × genotype) with repeated measurements (for the intensity variable). As expected, the main effect of intensity was significant ($P < 0.05$) for all measured parameters, and so only the effect of genotype and any significant interaction between the factors is reported in the text. Where ANOVA indicated a significant result, Bonferroni *post hoc* tests were used to evaluate

differences at individual intensities. The alpha level was set to 0.05. All data are reported as mean ± SEM. Student's *t*-test was used where indicated to compare saturating response amplitudes. All statistical comparisons were made using GRAPHPAD PRISM 4.0.

Results

Expression pattern of CAVIII protein in the mouse, rat and macaque retina

The localization pattern of CAVIII was examined by performing immunohistochemistry on vertical retinal sections from mice that were heterozygous or homozygous for the *wdl* mutation. CAVIII staining was present in the inner retina of the heterozygote mouse (Fig. 1A), but was absent from the retina of the homozygous *wdl* mutant mouse (Fig. 1B). Western blots of retinal and cerebellar lysates identified a single band at the predicted molecular weight of the CAVIII protein (~36 kDa) in C57BL6 wild-type mice that was not seen in the *wdl* mutant (Fig. 1C). We also compared the overall pattern of immunoreactivity in the rat (Fig. 1D) and macaque retina (Fig. 1E). The staining pattern was quite similar between species, with prominent immunoreactivity observed in bipolar cells with axon terminals stratifying in strata 5 of the ON sublamina, as well as in a small number of amacrine cell bodies. The pattern of CAVIII immunoreactivity in the mouse and macaque is described in further detail below.

CAVIII is localized to a subset of bipolar and amacrine cells in the mouse retina

Next, we wanted to determine the precise cellular localization of CAVIII in the C57BL6 mouse retina (Fig. 2), as this strain is more commonly used than the C57BLKS, the background strain of the *wdl* mice (shown in Fig. 1A). Overall, the staining intensity in the C57BL6 wild-type was higher than in the *wdl/+* mouse, particularly in the amacrine cell somata and processes in the inner plexiform layer (IPL), likely reflecting higher protein expression relative to the heterozygous mouse. Double-labeling for CAVIII and the RBC marker, PKC-α, revealed that the majority of CAVIII-positive cells were RBCs (Fig. 2A–D). CAVIII immunoreactivity was evident throughout the membrane of RBCs, with particularly bright staining in the axon terminal region. Weaker staining was observed in the cytoplasmic compartment.

An additional population of CAVIII-positive bipolar cells, that lacked PKC immunoreactivity, was observed in vertical sections and whole-mounts (Fig. 2D and G, arrowheads). These cells were less intensely stained compared with RBCs, appeared to lack cytoplasmic staining, and were positioned at a more proximal location in the inner nuclear layer (INL). Triple-staining showed that these cells were immunoreactive for secretagogin, a marker of cone-bipolar cells (Puthussery *et al.*, 2010). To identify the specific cone bipolar cell type that showed CAVIII immunoreactivity, we double-labeled for the vesicular glutamate transporter 1 (vGluT1), which labels all of the glutamatergic bipolar cell terminals in the IPL. We observed colocalization of vGluT1 and CAVIII in bipolar cell terminals located in the central region (strata 3) of the IPL (Fig. 2H–J, inset panels). Figure 3I shows CAVIII-positive processes co-stratifying and immediately proximal to the central calretinin band, which delineates the interface between strata 2 and 3 of the IPL. It is likely that the CAVIII-positive cone bipolar cells are Type 5 cells, as these cells are known to narrowly stratify in this region of the IPL (Ghosh *et al.*, 2004; Haverkamp *et al.*, 2009). Furthermore, staining for CAVIII in the Gustducin-GFP mouse retina revealed that the CAVIII-positive cone bipolar cells were not Type 7 bipolar cells, and double-labeling with Syt2, a marker of Type 2 and Type 6, cone bipolar cells showed no colocalization (data not shown).

In addition to bipolar cell staining, we observed a population of CAVIII-positive amacrine cells. To determine whether these cells use GABA or glycine as their principal

neurotransmitter, we double-labeled for CAVIII and GABA. Figure 3C and F shows that all CAVIII-positive cells were also stained for GABA. In contrast, we did not observe colocalization of CAVIII with glycine (data not shown). The intensity of GABA staining in the CAVIII-positive amacrine cells was quite variable, suggesting that a mixed population of amacrine cells expresses CAVIII. Moreover, the CAVIII-positive amacrine cells showed an irregular spatial distribution in the INL (Fig. 3F), providing further evidence for a heterogeneous population of GABAergic amacrine cells. Double-labeling for calretinin, a marker of starburst amacrine cells and another widefield GABAergic amacrine cell in mouse retina, showed no colocalization (Fig. 3G–I). Double-labeling with two additional markers of GABAergic amacrine cells, PKC-α and tyrosine hydroxylase, showed no colocalization (data not shown). Very occasionally, we observed CAVIII-positive displaced amacrine cells.

CAVII protein is localized to a subset of bipolar, amacrine and ganglion cells in the macaque retina

Because the CAVIII sequence is highly conserved amongst mammalian species, we examined the localization of this protein in the macaque retina. We observed CAVIII staining in a population of bipolar cells as well as in some amacrine and ganglion cells. To determine which bipolar cell types were CAVIII immunoreactive, we double-labeled for CAVIII and PKC-α in vertical sections and whole-mounts from a mid-peripheral region of the macaque retina. It should be noted that in the macaque, PKC-α labels the diffuse bipolar cell type DB4 in addition to RBCs (Grünert *et al.*, 1994). Most bipolar cells that were immunoreactive for CAVIII were RBCs (Fig. 4C and F); however, as in the mouse retina, an additional population of PKC-negative bipolar cells showed CAVIII immunoreactivity (Fig. 4A–F, arrowheads). These cells had smaller somata than RBCs, and also showed relatively lower CAVIII staining intensity in the cytoplasmic compartment. Double-labeling with CAVIII and secretagogin, a marker of the DB1 bipolar in macaque retina (Puthussery *et al.*, 2011), revealed that these PKC-negative bipolar cells were DB1 bipolar cells with axon terminals stratifying in the outer aspect of the IPL.

As in the mouse retina, CAVIII-positive amacrine cells were also immunoreactive for GABA (Fig. 5C and F). Some displaced CAV-III/GABA-positive amacrine cells were seen in the ganglion cell layer; however, these were relatively sparse compared with the density of CAVIII/GABA amacrine cells in the INL (Fig. 5I). In contrast to the mouse retina, we observed a population of large cell bodies in the ganglion cell layer that showed CAVIII immunoreactivity (Fig. 4C vertical section; Fig. 5G–I, whole-mount), but lacked GABA immunoreactivity (Fig. 5I), indicating that they were most likely ganglion cells. We observed two populations of putative ganglion cells, some showing strong CAVIII immunoreactivity and the others showing relatively weak staining. The average soma size (longest axis) of each of these populations of cells was very similar (bright cells, 18.4 + 0.4 μm; dim cells, 18.3 + 0.5 μm, n = 15–20). An average projection of one of the brightly stained CAVIII-positive ganglion cells is shown in Fig. 5J. A major dendritic projection is targeted to the OFF sublamina of the IPL, in the region of strata 2, indicating that these were OFF cells. We were unable to determine the precise level of stratification of the weakly stained ganglion cells.

We also noted the presence of CAVIII staining in the nerve fiber layer of the monkey whole-mount retina (Fig. 5K). CAVIII staining was visible along varicose ganglion cell axons, and high-power imaging revealed a higher density of CAVIII protein in the bulbous varicosities. Previous ultrastructural examination of these specializations showed a high density of mitochondria as well as desmosome and hemi-desmosome-like junctions between other axons and retinal glial cells (Wang *et al.*, 2003).

RBC light responses are normal in the CAVIII mutant mouse

All of the species that we examined showed robust expression of CAVIII in RBCs. Because some staining was present in the dendrites and soma, we considered the possibility that CAVIII could influence the mGluR6-mediated light responses in these cells. We made whole-cell patch-clamp recordings to measure flash-evoked responses in RBCs from *wdl* mutant mice and heterozygote littermates under voltage-clamp (V_{hold} = −70 mV) and current-clamp. RBCs were targeted by the characteristic position and shape of their somas. The identity of the recorded cells was confirmed by the presence of calcium-dependent inactivation of the light responses that is not present in ON cone bipolar cells (Berntson *et al.*, 2004; Puthussery *et al.*, 2009).

The amplitude and kinetics of average RBC current responses evoked by light flashes ranging in intensity from 0.34 photons/μm^2 to 94 photons/μm^2 were essentially indistinguishable between *wdl* mutants (Fig. 6A; red traces, n = 12 cells, five mice) and heterozygote mice (black traces, n = 8 cells, five mice). Two-way ANOVA (intensity × genotype) showed no main effect of genotype on total charge transfer (Fig. 6B; $F_{8,1}$ = 0.44, P = 0.51), delay to half-maximum amplitude (Fig. 6C; $F_{5,1}$ = 0.16, P = 0.74) or the response half-width (Fig. 6D; $F_{5,1}$ = 0.10, P = 0.76). It should be noted that the delay and half-width measurements could only be reliably made for the six highest stimulus intensities as there were response failures at the lowest three intensities that were tested. The amplitudes of the RBC current responses for a near-saturating stimulus intensity were not statistically different between genotypes (*wdl*/+, −164 ± 5 pA; *wdl*/*wdl*, −154 ± 5 pA; *t*-test, P = 0.19), and were similar to previously published values in other mouse lines (Berntson *et al.*, 2004; Puthussery *et al.*, 2010).

We also evaluated the light-evoked voltage response under current-clamp (Fig. 6E). Overall, the *wdl* mutation did not significantly affect the peak voltage response (two-way ANOVA, $F_{8,1}$ = 0.21, P = 0.65). At the highest stimulus intensity, the average peak voltage responses were comparable at 29 ± 4 mV for the *wdl*/+ and 28 ± 2 mV for the *wdl*/*wdl* mice. The delay to half-maximum amplitude (Fig. 6G; two-way ANOVA, $F_{6,1}$ = 0.03, P = 0.86) and the response half-width (Fig. 6H; two-way ANOVA, $F_{6,1}$ = 4.40, P = 0.0504) were also unaffected by the *wdl* mutation. A comparison of the response half-width at the maximal flash intensity was not statistically significant (*wdl*/+, 402 ± 25 ms; *wdl*/*wdl*, 477 ± 31 ms, *t*-test, P = 0.10).

Overall, the loss of functional CAVIII had no significant effect on transmission from the rod photoreceptors to the RBCs, nor was there any effect on the mGluR6-mediated response.

The AII-AC response is prolonged in the CAVIII mutant mouse

Given the strong immunoreactivity for CAVIII in the axon terminals of RBCs, we investigated whether CAVIII could influence transmitter release at the RBC axon terminal, thereby altering the responses of the postsynaptic neurons (Fig. 7). Because the AII-AC is postsynaptic to the RBC ribbon dyad, we measured light-evoked currents from these neurons in the *wdl* mutant (Fig. 7A; red traces, n = 10, four mice) and heterozygous littermates (black traces, n = 10, four mice). Overall, the AII-AC responses from the *wdl* mutant mice were larger in amplitude and more sustained compared with the littermate controls. The total charge transfer was significantly higher in the *wdl* mutant (Fig. 7B; two-way anova, $F_{8,1}$ = 8.86, P = 0.01) and there was a significant interaction between intensity and genotype ($F_{8,1}$ = 3.48, P = 0.001), indicating that the charge difference was more marked for higher stimulus intensities. For the highest flash intensity, the charge transfer was approximately twofold larger in the *wdl* mutant (91 ± 15 pC) compared with control (42 ± 10 pC). The responses from the *wdl* mutant were also more prolonged compared with the

control group, as shown by the differences in the measured response half-width (Fig. 7C; two-way ANOVA, $F_{8,1} = 8.86$, $P = 0.008$). For the four highest stimulus intensities, *wdl*/*wdl* responses lasted, on average, ~40% longer than the control responses (Fig. 7D).

A comparison of the time course of the normalized AII-AC responses is shown for sub-saturating (Fig. 7C1) and saturating responses (Fig. 7C2). At sub-saturating intensities, the time course of the normalized AII-AC response was more prolonged in the *wdl* mutant compared with the control. For the saturating stimulus, the normalized response in the AII-AC was more prolonged than the voltage response in RBCs at the same light intensity (Fig. 7C2, grey), and it was relatively more prolonged in the *wdl* mutant than in control animals, indicating that differences in response amplitude cannot account for the differing response time course. At higher stimulus intensities, the time course of the AII-AC EPSCs was characterized by a rapid rise to an initial peak, followed by a slight decline (nose in the response), followed by a slower secondary rising phase. This behavior is most evident in individual responses (Fig. 8A), but can also be discerned in the average responses (Fig. 7A and C2, red trace). Previous work has distinguished similar fast and slow components to the time course of the AII EPSCs (Nelson, 1982; Dacheux & Raviola, 1986; Bloomfield & Xin, 2000; Trexler *et al.*, 2005). Neither the time-to-half-peak nor the initial rate of rise of AII-AC EPSCs differed significantly between control and mutant animals (data not shown). Thus, the major effect of the absence of CAVIII was to prolong the AII-AC EPSCs, with little effect on the rising phase of the responses. The results suggest that without CAVIII, the release of transmitter from the RBCs is larger and longer, indicating that CAVIII is important for terminating transmitter release, particularly at high stimulus intensities.

AII-ACs are known to be electrically coupled to each other via gap junctions, and the extent of this coupling is determined by the adaptation state of the retina (Hampson *et al.*, 1992; Baldridge *et al.*, 1998; Bloomfield & Volgyi, 2004; Kothmann *et al.*, 2009). Under low-scotopic and high-photopic conditions, the AII-AC network is minimally coupled, whereas over much of the intermediate operating range, the network becomes more extensively coupled. When coupling is strong, adjacent AII-ACs can contribute a slow component of the light-evoked EPSC that does not reverse at positive voltages (Trexler *et al.*, 2005). We measured light-evoked current–voltage relations in *wdl* AII-ACs to determine whether the prolonged response kinetics seen in the *wdl* mutant could have been generated by increased gap junctional coupling (Fig. 8A and B). We found that the light-evoked current–voltage relation was linear between −80 and +60 mV, and reversed at ~0 mV (Fig. 8C), as expected for α-amino-3-hydroxy-5-methyl-4-isoxazolepropionic acid (AMPA)-mediated glutamatergic inputs, and inconsistent with the notion that the prolonged response in the *wdl* mutant results from increased coupling in the AII-AC network.

Calcium currents of RBCs in the wdl mutant

We considered the possibility that the extended duration of the AII-AC response might reflect changes in activation of calcium channels in RBC axon terminals. Previous immunohistochemical and physiological studies have shown that RBCs express L-type channels at their axon terminals (Protti & Llano, 1998; Morgans, 2001; Berntson *et al.*, 2003). T-type channels have also been reported in RBCs, and may contribute to glutamate release (Pan, 2000; Pan *et al.*, 2001; Hu *et al.*, 2009). We compared the calcium currents in *wdl* mutant and heterozygote animals (Fig. 9). Outward potassium currents were suppressed by intracellular Cs, and synaptic inhibition was blocked by inclusion of strychnine, picrotoxin and TPMPA in the bath solution. L-type currents were selectively activated from a holding potential of −70 mV, a potential at which the T-type channels are largely inactivated (see below). The amplitude and time course (Fig. 9A), and the current–voltage relations of the L-type currents (Fig. 9C) were indistinguishable between the two groups.

From a holding potential of −100 mV, a series of depolarizing pulses produced the additional activation of a low-threshold inward current that inactivated rapidly during the voltage pulse (Fig. 9B). This additional current is consistent with activation of T-type calcium channels that have been previously characterized in these cells (Pan, 2000; Pan *et al.*, 2001). The magnitude and time course of the total calcium current was identical in the wild-type and mutant animals (Fig. 9B). Analysis of the steady-state inactivation of the T-type component indicated that it became half-inactivated at ~−80 mV (Fig. 9E), in agreement with previous data (Perez-Reyes, 2003). The inactivation properties of the T-type calcium channels were unchanged in the mutant animal (Fig. 9E). Thus, the changes observed in the AII-AC EPSC in *wdl* mutants cannot be accounted for by changes in the amplitude or kinetics of voltage-activated calcium currents in the presynaptic RBC terminals.

Synaptic connectivity and density of RBCs is normal in the CAVIII mutant

Alterations in synaptic organization have been observed in the cerebellum of *wdl* mutant mice. Therefore, we evaluated the synapses of RBCs in the inner and outer plexiform layer (OPL) of the *wdl* mutant. In the OPL, glutamate released by rod photoreceptors activates mGluR6 receptors, which are localized to the tips of the invaginating RBC dendrites. To assess whether this synaptic organization was preserved in the mutant mouse, we triple-labeled retinas from *wt* and *wdl* mice for the ribbon marker RIBEYE, as well as PKC and mGluR6 (Fig. 10). No abnormalities were observed in the RBC dendrites; similar to the wild-type retina, the mGluR6 receptors were located at the dendritic tips and were found in close proximity to the ribbon synapses. Furthermore, in the inner retina, the axon terminals of the RBCs showed normal localization of RIBEYE, suggesting that the phenotype observed in the AII-ACs could not be attributed to gross alterations in synaptic ribbon density or localization. Finally, the density of RBCs in the mutant mouse was not significantly different to heterozygote littermates (15 533 ± 446/mm^2 in *wdl*/+ and 15 712 ± 607/mm^2 in *wdl*/*wdl*, *t*-test, $P = 0.82$). These densities accord well with values reported previously in the mouse retina (Wässle *et al.*, 2009). Thus, mutation of the *Car8* gene does not alter the overall density of RBCs.

We also performed electron microscopy to evaluate the ultrastructural integrity of the RBC to AII-AC synapse in the *wdl* mutant mouse (Fig. 11). RBC axon terminals could be readily identified by their large size and close proximity to the ganglion cell layer. The synaptic ribbons in the RBC axon terminal of the *wdl* mice were of normal size and appeared to be docked to the plasma membrane. Moreover, the terminals had a high density of synaptic vesicles, some of which were docked to the synaptic ribbon. Putative AII-AC and A17 amacrine cell processes were evident at the synaptic ribbons. These data indicate that gross changes in ultrastructure of the RBC axon terminal do not underlie the observed functional phenotype in the *wdl* mouse.

Discussion

The data demonstrate selective expression of CAVIII protein in RBCs, and some GABAergic amacrine cells, that is conserved in several mammalian retinas. In agreement with the immunohistochemical localization of CAVIII to RBCs, and the strong staining of the axon terminals, mutant mice lacking CAVIII showed alterations in synaptic transmission from the RBCs to the AII-ACs. These changes were unlikely to be due to changes in the input to RBCs as the mGluR6-mediated light-evoked currents and voltage responses were normal. Moreover, the results could not be accounted for by changes in synaptic ultrastructure or by alterations in the activation or inactivation of voltage-gated calcium channels in the RBC axon terminal.

Localization of CAVIII in RBCs of the mammalian retina

The expression of CAVIII in Purkinje cells is conserved in phylogenetically diverse species, including zebrafish (Bae *et al.*, 2009), mice and monkeys (Jiao *et al.*, 2005). Similarly, in this study, we observed conserved localization of CAVIII in RBCs. CAVIII protein was also observed in subsets of amacrine cells in all of these species; however, screening with known GABAergic amacrine cell markers did not provide unequivocal identification. Thus, whether CAVIII is expressed in homologous amacrine cells remains to be determined. Although the presence of CAVIII-immunoreactive RBCs and GABAergic amacrine cells was seen in all species that we examined, some variability was seen amongst the type of cone bipolar cells that were labeled with this protein. In mouse retina, CAVIII labeled cone bipolar cells with axon terminals ending in strata 3 of the IPL, which were most likely Type 5 ON cone bipolars. In contrast, in monkey retina, CAVIII labeled an OFF cone bipolar cell type. Another notable species difference was that CAVIII was present in ganglion cells only in the macaque retina. The protein was localized to the soma, dendrites and axons of at least two large ganglion cell types, one of which was clearly distinguishable as an OFF cell. The large soma size and relatively high density of these cells suggests that they could be parasol ganglion cells. It is of interest to note that *Car10*, another acatalytic CA, is enriched in cone bipolar cells of the mouse retina (Kim *et al.*, 2008; Nakajima *et al.*, 2009). Further studies will be necessary to elucidate the function of CAVIII in amacrine and ganglion cells, and to investigate the expression and function of *Car10*.

The wdl mutation does not affect the density or synaptic ultrastructure of RBCs

Purkinje cells in the *wdl* mutant have a reduced number of inputs from parallel fibers and an increased number of free dendritic spines, suggesting that CAVIII is important for synaptic development and/or maintenance (Hirasawa *et al.*, 2007). In contrast, our data indicate that the absence of CAVIII does not alter synaptic input to RBCs, as synaptic organization, as well as light-evoked responses, were normal in these cells. Moreover, our results indicate that CAVIII is not involved in the developmental regulation of RBC density. Because the absence of CAVIII did not alter the expression of RIBEYE or the overall ultrastuctural organization of the RBC axon terminal, it is unlikely that gross structural alterations in the ribbon synapse underlie the functional phenotype that we observed in the *wdl* mutants. However, it remains possible that other more subtle alterations could contribute to changes in signaling at this synapse.

The wdl mutation alters light-evoked AII-AC responses

A key finding was the occurrence of larger, more prolonged AII-AC EPSCs in the *wdl* mouse. The effect could not be accounted for by changes in the RBC light response, suggesting that the site of CAVIII activity is most likely to be at the RBC axon terminal, where CAVIII protein is most abundantly localized. Results from cerebellar Purkinje cells may provide clues to a mechanism for this altered postsynaptic response in the AII-AC. Hirota *et al.* (2003) demonstrated a direct interaction between CAVIII and IP3R1, and demonstrated that CAVIII acts as a negative regulator of IP3R1 by reducing the affinity of the IP3R1 receptor for IP3. IP3R1 and CAVIII are abundantly expressed and colocalized in cerebellar Purkinje cells; however, normal levels of IP3R1 are present in the cerebellum of the *wdl* mutant mouse in the absence of CAVIII (Jiao *et al.*, 2005). If CAVIII normally inhibited binding of IP3 to IP3R1, its absence could increase the release of calcium from IP3-sensitive intracellular stores. Such a mechanism has been proposed to underlie the ataxic phenotype observed in the *wdl* mutant (Jiao *et al.*, 2005; Turkmen *et al.*, 2009); however, direct functional evidence is lacking. In this context, it is interesting to note that IP3Rs have been localized to RBC axon terminals in the mouse and rat retina (Peng *et al.*, 1991; Micci & Christensen, 1996; Koulen *et al.*, 2005), and functional IP3R1 channels in RBCs have been documented (Koulen *et al.*, 2005).

Another possibility is that CAVIII alters RBC transmitter release, through another as yet unidentified mechanism. Gene array studies of the cerebellums of *wdl* mutants have revealed alterations in clusters of genes associated with vesicle assembly and transport, signal transduction and synaptogenesis (Yan *et al.*, 2007). Interestingly, the gene encoding the presynaptic cytomatrix protein, Piccolo, a protein involved in trafficking of synaptic vesicles to the active zone, is downregulated in the cerebellum of *wdl* mutants. Piccolo is a known component of bipolar cell ribbon synapses. Although our ultrastructural studies failed to reveal any gross alterations in vesicle number in RBC axon terminals, it is possible that other proteins involved in vesicle trafficking could be altered in these mutants.

Because the CAVIII protein is localized to the RBC axon and not on the AII-AC, it seems most likely that the phenotype observed here arises from changes originating in the RBC axon terminal, rather than the AII-AC. However, it is possible that mutation-induced changes in transmitter release from the RBC terminal could lead to homeostatic plasticity in the postsynaptic glutamate receptors that are expressed on the AII-AC. Several studies have demonstrated that transmission from the RBC to the AII-AC is mediated by AMPA receptors (Morkve *et al.*, 2002; Singer & Diamond, 2003; Veruki *et al.*, 2003). If the absence of CAVIII reduced synaptic release of glutamate, it is possible that this could lead to increased surface expression and miniature EPSC amplitudes of the postsynaptic AMPA receptors, as has been shown previously under conditions of reduced neuronal activity (O'Brien *et al.*, 1998; Shepherd *et al.*, 2006).

Prior analyses have concluded that transmitter release at mammalian RBC terminals results from calcium influx close to active channels, and that release from RBCs should closely track calcium channel activity (Jarsky *et al.*, 2010; Oltedal & Hartveit, 2010). Because calcium channel kinetics are very rapid compared with light-driven responses, the transmitter release from RBCs should closely track the RBC membrane potential. Such a model is difficult to reconcile with the effect of CAVIII mutation on RBC synaptic transmission, as the duration of the AII-AC EPSCs was significantly prolonged in the mutant, while the duration of the RBC voltage response was unaffected. Moreover, the characteristic kinetics of the AII-AC EPSC, with an initial rapid rise, followed by a slower secondary component, does not appear to reflect the RBC voltage response in either the wild-type or mutant. Previous recordings have identified two components of release from RBCs, an initial fast transient component that is depleted within a few milliseconds and a slower sustained component that is depleted over several hundred milliseconds (Zhou *et al.*, 2006; Oltedal & Hartveit, 2010). These components are proposed to reflect release from a 'rapidly releasing pool' of vesicles that are docked and primed at the active zone, and a 'releasable pool or reserve pool' of vesicles that are primed further up the ribbon, respectively (for review, see Wan & Heidelberger, 2011).

An alternative explanation for the slow phase of the EPSCs observed in AII-ACs is not presynaptic but postsynaptic; AII-ACs are extensively coupled under some conditions, and the slow component might comprise a filtered signal originating in coupled cells (Singer & Diamond, 2003). Such coupling is evident in a recorded cell as a nonlinearity in the current–voltage relation and an inability to reverse the inward current at positive potentials (Trexler *et al.*, 2005). Our voltage-clamp experiments indicate that, under our recording conditions, the slow component cannot be accounted for by filtered input from adjacent gap-junction-coupled cells, because the current–voltage relation was linear and reversed at 0 mV, as expected for an AMPA-mediated input. Thus, the prolonged AII-AC EPSC in the *wdl* mutant is more consistent with an enhancement of a slower, sustained component of release from RBCs.

In summary, the results are in line with other work (Snellman *et al.*, 2009), and indicate that transmitter release from RBCs during physiological stimulation may not simply reflect calcium channel activity at active zones, but more likely reflects more complex intra-terminal calcium dynamics that drive terminal vesicle cycling (Wan & Heidelberger, 2011). The enhanced sustained response component suggests, that under normal conditions, CAVIII may serve to curtail transmitter release, particularly during strong stimulation, and thus may contribute to mechanisms that control the synaptic gain.

Acknowledgments

This research was supported by National Eye Institute Grant #EY017095 (W.R.T.), a National Health and Medical Research Council (Australia) PostDoctoral Fellowship #520033 (T.P.), an Unrestricted grant from Research to Prevent Blindness (Department of Ophthalmology, OHSU) and the Neuroscience Imaging Center (P30-NS06180) and Opthalmology Core Facility (5P30-EY010572-17) at OHSU. We thank Prof. Takahisa Furukawa for generously providing the mGluR6 antibody.

Abbreviations

AII-AC	AII-amacrine cell
AMPA	α-amino-3-hydroxy-5-methyl-4-isoxazole-propionic acid
CA	carbonic anhydrase
CAVIII	carbonic anhydrase-related protein VIII
EPSC	excitatory postsynaptic current
GABA	γ-aminobutyric acid
IB	incubation buffer
INL	inner nuclear layer
IP3R1	IP3 receptor type 1
IPL	inner plexiform layer
OPL	outer plexiform layer
PBS	phosphate-buffered saline
PKC-α	protein kinase C, alpha subunit
RBC	rod bipolar cell
Tx-100	Triton X-100
vGluT1	vesicular glutamate transporter 1

References

Aspatwar A, Tolvanen ME, Parkkila S. Phylogeny and expression of carbonic anhydrase-related proteins. BMC Mol Biol. 2010; 11:25. [PubMed: 20356370]

Bae YK, Kani S, Shimizu T, Tanabe K, Nojima H, Kimura Y, Higashijima S, Hibi M. Anatomy of zebrafish cerebellum and screen for mutations affecting its development. Dev Biol. 2009; 330:406–426. [PubMed: 19371731]

Baldridge WH, Vaney DI, Weiler R. The modulation of intercellular coupling in the retina. Semin Cell Dev Biol. 1998; 9:311–318. [PubMed: 9665867]

Berntson A, Taylor WR, Morgans CW. Molecular identity, synaptic localization, and physiology of calcium channels in retinal bipolar cells. J Neurosci Res. 2003; 71:146–151. [PubMed: 12478624]

Berntson A, Smith RG, Taylor WR. Postsynaptic calcium feedback between rods and rod bipolar cells in the mouse retina. Vis Neurosci. 2004; 21:913–924. [PubMed: 15733346]

Bloomfield SA, Volgyi B. Function and plasticity of homologous coupling between AII amacrine cells. Vision Res. 2004; 44:3297–3306. [PubMed: 15535997]

Bloomfield SA, Xin D. Surround inhibition of mammalian AII amacrine cells is generated in the proximal retina. J Physiol. 2000; 523:771–783. [PubMed: 10718754]

Burns ME, Mendez A, Chen J, Baylor DA. Dynamics of cyclic GMP synthesis in retinal rods. Neuron. 2002; 36:81–91. [PubMed: 12367508]

Dacheux RF, Raviola E. The rod pathway in the rabbit retina: a depolarizing bipolar and amacrine cell. J Neurosci. 1986; 6:331–345. [PubMed: 3950701]

Dodt HU, Eder M, Schierloh A, Zieglgansberger W. Infrared-guided laser stimulation of neurons in brain slices. Sci STKE. 2002:l2.

Ghosh KK, Bujan S, Haverkamp S, Feigenspan A, Wässle H. Types of bipolar cells in the mouse retina. J Comp Neurol. 2004; 469:70–82. [PubMed: 14689473]

Grünert U, Martin PR, Wässle H. Immunocytochemical analysis of bipolar cells in the macaque monkey retina. J Comp Neurol. 1994; 348:607–627. [PubMed: 7530731]

Hampson EC, Vaney DI, Weiler R. Dopaminergic modulation of gap junction permeability between amacrine cells in mammalian retina. J Neurosci. 1992; 12:4911–4922. [PubMed: 1281499]

Haverkamp S, Inta D, Monyer H, Wässle H. Expression analysis of green fluorescent protein in retinal neurons of four transgenic mouse lines. Neuroscience. 2009; 160:126–139. [PubMed: 19232378]

Hirasawa M, Xu X, Trask RB, Maddatu TP, Johnson BA, Naggert JK, Nishina PM, Ikeda A. Carbonic anhydrase related protein 8 mutation results in aberrant synaptic morphology and excitatory synaptic function in the cerebellum. Mol Cell Neurosci. 2007; 35:161–170. [PubMed: 17376701]

Hirota J, Ando H, Hamada K, Mikoshiba K. Carbonic anhydrase-related protein is a novel binding protein for inositol 1,4,5-trisphosphate receptor type 1. Biochem J. 2003; 372:435–441. [PubMed: 12611586]

Hu C, Bi A, Pan ZH. Differential expression of three T-type calcium channels in retinal bipolar cells in rats. Vis Neurosci. 2009; 26:177–187. [PubMed: 19275782]

Jarsky T, Tian M, Singer JH. Nanodomain control of exocytosis is responsible for the signaling capability of a retinal ribbon synapse. J Neurosci. 2010; 30:11885–11895. [PubMed: 20826653]

Jiao Y, Yan J, Zhao Y, Donahue LR, Beamer WG, Li X, Roe BA, Ledoux MS, Gu W. Carbonic anhydrase-related protein VIII deficiency is associated with a distinctive lifelong gait disorder in waddles mice. Genetics. 2005; 171:1239–1246. [PubMed: 16118194]

Kato K. Sequence of a novel carbonic anhydrase-related polypeptide and its exclusive presence in Purkinje cells. FEBS Lett. 1990; 271:137–140. [PubMed: 2121526]

Kim DS, Ross SE, Trimarchi JM, Aach J, Greenberg ME, Cepko CL. Identification of molecular markers of bipolar cells in the murine retina. J Comp Neurol. 2008; 507:1795–1810. [PubMed: 18260140]

Koike C, Obara T, Uriu Y, Numata T, Sanuki R, Miyata K, Koyasu T, Ueno S, Funabiki K, Tani A, Ueda H, Kondo M, Mori Y, Tachibana M, Furukawa T. TRPM1 is a component of the retinal ON bipolar cell transduction channel in the mGluR6 cascade. Proc Natl Acad Sci USA. 2010; 107:332–337. [PubMed: 19966281]

Kothmann WW, Massey SC, O'Brien J. Dopamine-stimulated dephosphorylation of connexin 36 mediates AII amacrine cell uncoupling. J Neurosci. 2009; 29:14903–14911. [PubMed: 19940186]

Koulen P, Wei J, Madry C, Liu J, Nixon E. Differentially distributed IP3 receptors and Ca^{2+} signaling in rod bipolar cells. Invest Ophthalmol Vis Sci. 2005; 46:292–298. [PubMed: 15623787]

Lakkis MM, O'Shea KS, Tashian RE. Differential expression of the carbonic anhydrase genes for CA VII (Car7) and CA-RP VIII (Car8) in mouse brain. J Histochem Cytochem. 1997; 45:657–662. [PubMed: 9154152]

Micci MA, Christensen BN. Distribution of the inositol trisphosphate receptor in the catfish retina. Brain Res. 1996; 720:139–147. [PubMed: 8782906]

Morgans CW. Localization of the alpha(1F) calcium channel subunit in the rat retina. Invest Ophthalmol Vis Sci. 2001; 42:2414–2418. [PubMed: 11527958]

Morkve SH, Veruki ML, Hartveit E. Functional characteristics of non-NMDA-type ionotropic glutamate receptor channels in AII amacrine cells in rat retina. J Physiol. 2002; 542:147–165. [PubMed: 12096058]

Nakajima Y, Moriyama M, Hattori M, Minato N, Nakanishi S. Isolation of ON bipolar cell genes via hrGFP-coupled cell enrichment using the mGluR6 promoter. J Biochem. 2009; 145:811–818. [PubMed: 19270057]

Nelson R. AII amacrine cells quicken time course of rod signals in the cat retina. J Neurophysiol. 1982; 47:928–947. [PubMed: 6177841]

O'Brien RJ, Kamboj S, Ehlers MD, Rosen KR, Fischbach GD, Huganir RL. Activity-dependent modulation of synaptic AMPA receptor accumulation. Neuron. 1998; 21:1067–1078. [PubMed: 9856462]

Oltedal L, Hartveit E. Transient release kinetics of rod bipolar cells revealed by capacitance measurement of exocytosis from axon terminals in rat retinal slices. J Physiol. 2010; 588:1469–1487. [PubMed: 20211976]

Pan ZH. Differential expression of high- and two types of low-voltage-activated calcium currents in rod and cone bipolar cells of the rat retina. J Neurophysiol. 2000; 83:513–527. [PubMed: 10634892]

Pan ZH, Hu HJ, Perring P, Andrade R. T-type Ca(2^+) channels mediate neurotransmitter release in retinal bipolar cells. Neuron. 2001; 32:89–98. [PubMed: 11604141]

Peng YW, Sharp AH, Snyder SH, Yau KW. Localization of the inositol 1,4,5-trisphosphate receptor in synaptic terminals in the vertebrate retina. Neuron. 1991; 6:525–531. [PubMed: 1849721]

Perez-Reyes E. Molecular physiology of low-voltage-activated t-type calcium channels. Physiol Rev. 2003; 83:117–161. [PubMed: 12506128]

Protti DA, Llano I. Calcium currents and calcium signaling in rod bipolar cells of rat retinal slices. J Neurosci. 1998; 18:3715–3724. [PubMed: 9570802]

Puthussery T, Gayet-Primo J, Taylor WR. Localization of the calcium-binding protein secretagogin in cone bipolar cells of the mammalian retina. J Comp Neurol. 2010; 518:513–525. [PubMed: 20020539]

Puthussery T, Gayet-Primo J, Taylor WR. Immunohistochemical identification and synaptic inputs to the diffuse bipolar cell type DB1 in macaque retina. J Comp Neurol. 201110.1002/cne.22756

Puthussery T, Gayet-Primo J, Pandey S, Duvoisin RM, Taylor WR. Differential loss and preservation of glutamate receptor function in bipolar cells in the rd10 mouse model of retinitis pigmentosa. Eur J Neurosci. 2009; 29:1533–1542. [PubMed: 19385989]

Shepherd JD, Rumbaugh G, Wu J, Chowdhury S, Plath N, Kuhl D, Huganir RL, Worley PF. Arc/Arg3.1 mediates homeostatic synaptic scaling of AMPA receptors. Neuron. 2006; 52:475–484. [PubMed: 17088213]

Singer JH, Diamond JS. Sustained Ca^{2+} entry elicits transient postsynaptic currents at a retinal ribbon synapse. J Neurosci. 2003; 23:10923–10933. [PubMed: 14645488]

Sjoblom B, Elleby B, Wallgren K, Jonsson BH, Lindskog S. Two point mutations convert a catalytically inactive carbonic anhydrase-related protein (CARP) to an active enzyme. FEBS Lett. 1996; 398:322–325. [PubMed: 8977131]

Skaggs LA, Bergenhem NC, Venta PJ, Tashian RE. The deduced amino acid sequence of human carbonic anhydrase-related protein (CARP) is 98% identical to the mouse homologue. Gene. 1993; 126:291–292. [PubMed: 8482548]

Snellman J, Zenisek D, Nawy S. Switching between transient and sustained signalling at the rod bipolar-AII amacrine cell synapse of the mouse retina. J Physiol. 2009; 587:2443–2455. [PubMed: 19332496]

Trexler EB, Li W, Massey SC. Simultaneous contribution of two rod pathways to AII amacrine and cone bipolar cell light responses. J Neurophysiol. 2005; 93:1476–1485. [PubMed: 15525810]

Turkmen S, Guo G, Garshasbi M, Hoffmann K, Alshalah AJ, Mischung C, Kuss A, Humphrey N, Mundlos S, Robinson PN. CA8 mutations cause a novel syndrome characterized by ataxia and mild mental retardation with predisposition to quadrupedal gait. PLoS Genet. 2009; 5:e1000487. [PubMed: 19461874]

Venkataramani S, Taylor WR. Orientation selectivity in rabbit retinal ganglion cells is mediated by presynaptic inhibition. J Neurosci. 2010; 30:15664–15676. [PubMed: 21084622]

Veruki ML, Morkve SH, Hartveit E. Functional properties of spontaneous EPSCs and non-NMDA receptors in rod amacrine (AII) cells in the rat retina. J Physiol. 2003; 549:759–774. [PubMed: 12702738]

Wan QF, Heidelberger R. Synaptic release at mammalian bipolar cell terminals. Vis Neurosci. 2011; 28:109–119. [PubMed: 21272392]

Wang L, Dong J, Cull G, Fortune B, Cioffi GA. Varicosities of intraretinal ganglion cell axons in human and nonhuman primates. Invest Ophthalmol Vis Sci. 2003; 44:2–9. [PubMed: 12506048]

Wässle H, Puller C, Muller F, Haverkamp S. Cone contacts, mosaics, and territories of bipolar cells in the mouse retina. J Neurosci. 2009; 29:106–117. [PubMed: 19129389]

Winsky L, Isaacs KR, Jacobowitz DM. Calretinin mRNA and immunoreactivity in the medullary reticular formation of the rat: colocalization with glutamate receptors. Brain Res. 1996; 741:123–133. [PubMed: 9001714]

Yan J, Jiao Y, Jiao F, Stuart J, Donahue LR, Beamer WG, Li X, Roe BA, LeDoux MS, Gu W. Effects of carbonic anhydrase VIII deficiency on cerebellar gene expression profiles in the wdl mouse. Neurosci Lett. 2007; 413:196–201. [PubMed: 17174474]

Zhou ZY, Wan QF, Thakur P, Heidelberger R. Capacitance measurements in the mouse rod bipolar cell identify a pool of releasable synaptic vesicles. J Neurophysiol. 2006; 96:2539–2548. [PubMed: 16914610]

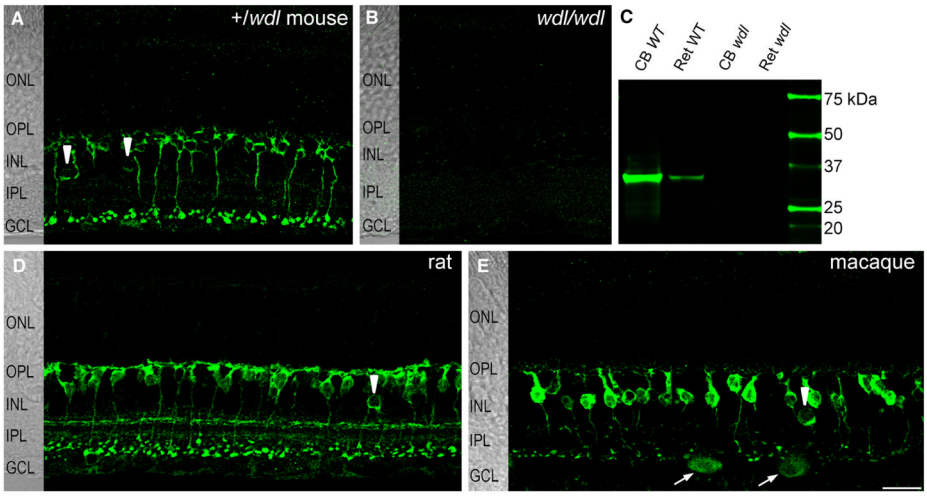

Fig. 1.

CAVIII immunoreactivity is similar between mammalian species and is absent from the *wdl* mouse. CAVIII immunoreactivity in vertical sections of retina from the *wdl*/+ mouse (A), *wdl*/*wdl* mouse (B), rat (D) and (E) macaque retina. All images are average projections of confocal stacks. The retinal layers are shown on transmitted light images to the left of each panel. In heterozygous mice (A), prominent CAVIII immunoreactivity is seen in the inner retina. No staining was detectable in retina from the homozygous *wdl* mutant (B). In all species, CAVIII immunoreactivity is present in a subset of bipolar cells with axon terminals stratifying in the innermost region of the IPL and in some amacrine cell somata (arrowheads in A, D and E). In the macaque retina, some putative ganglion cells are also stained (arrows). (C) Western blot of cerebellar (15 μg) and retinal (30 μg) lysates from C57BL6 wild-type and *wdl* mouse probed with an antibody for CAVIII. A single band is observed at the predicted molecular weight of ~36 kDa in wild-type tissues that is absent from the *wdl* mutant. Scale bars: 20 μm. CB, cone bipolar; GCL, ganglion cell layer; INL, inner nuclear layer; IPL, inner plexiform layer; ONL, outer nuclear layer; OPL, outer plexiform layer; WT, wild-type.

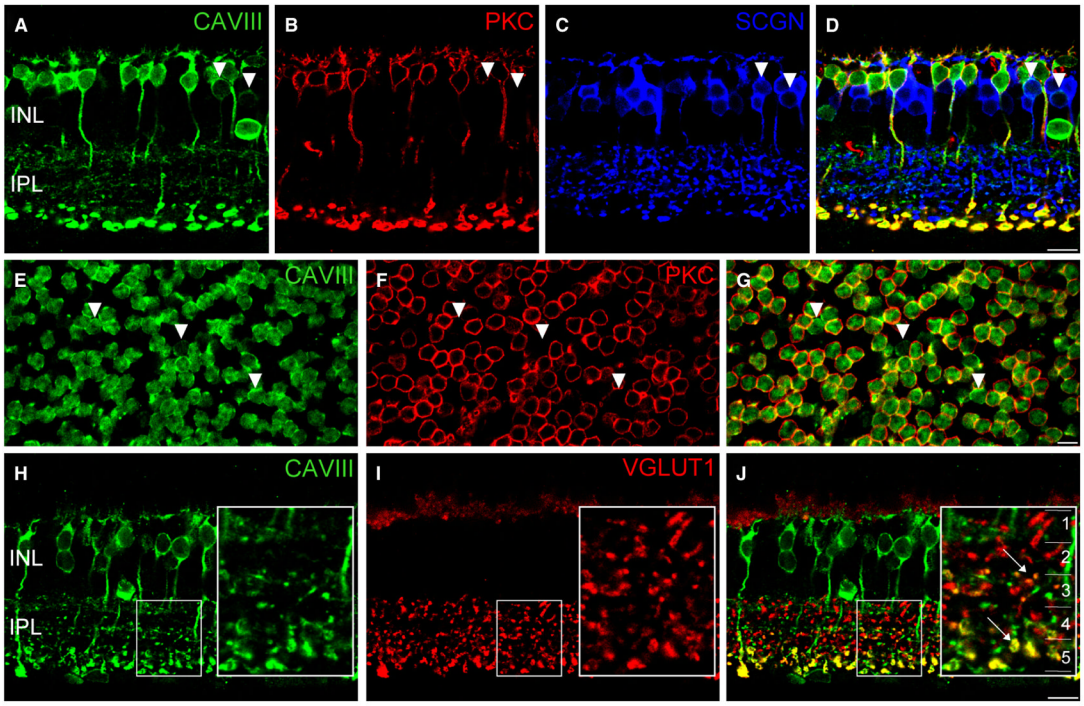

Fig. 2.

CAVIII is localized to rod bipolar cells (RBCs) and a subset of cone bipolar cells in the wild-type mouse retina. (A–D) Triple-labeling for CAVIII, the RBC marker, PKC and the cone bipolar cell marker, SCGN in a vertical section of the mouse retina. Merged image shown in (D). Most CAVIII-positive bipolar cells colocalize with PKC; however, those lacking PKC colocalize with SCGN, indicating that they are cone bipolar cells (arrowheads). (E–G) Staining of a mouse retinal whole-mount labeled for CAVIII and PKC, focused at the level of the proximal INL. Merged image shown in (G). As in vertical sections, most CAVIII-positive bipolar cells are PKC positive, whilst a smaller number are PKC negative (arrowheads). (H–J) Vertical section labeled for CAVIII and vGluT1. The inset shows a magnified view of the region defined by the dotted rectangle. The inset in (C) shows the five strata (1–5) of the IPL. CAVIII colocalizes with vGluT1 in the middle region of the IPL (S3), as well as in S5 where the RBCs stratify (arrows). Scale bars: 10 μm. CAVIII, carbonic anhydrase-related protein VIII; INL, inner nuclear layer; IPL, inner plexiform layer; PKC, protein kinase C; SCGN, secretagogin; vGluT1, vesicular glutamate transporter 1.

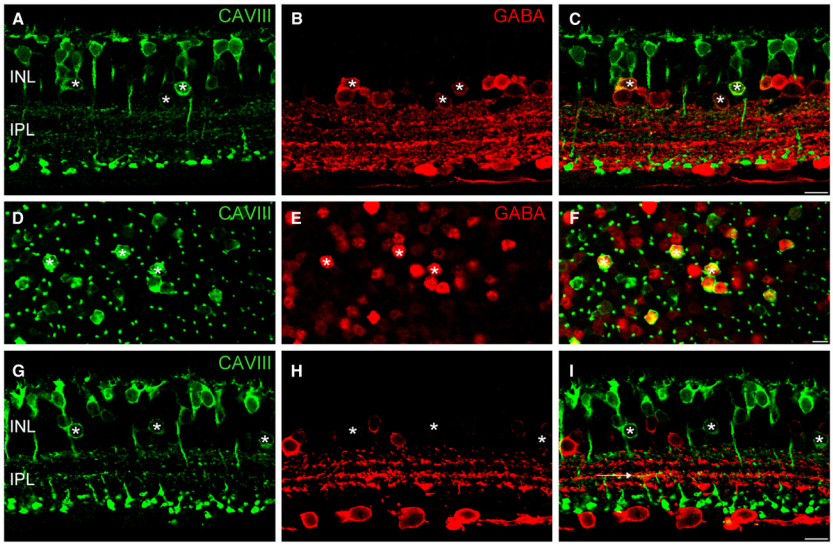

Fig. 3.

CAVIII is localized to a subset of GABAergic amacrine cells in the wild-type mouse retina. (A–F) Immunolocalization of CAVIII (green) and GABA (red) in vertical section (A–C) and whole-mount (D–F) of the mouse retina. All CAVIII-positive amacrine cells are also immunoreactive for GABA (*). The spatial distribution of CAVIII-positive amacrine cells is irregular, and the intensity of GABA staining in these cells is variable, suggesting that a heterogeneous population of GABAergic amacrine cells express CAVIII. (G–I) CAVIII-positive amacrine cells (*) do not show calretinin immunoreactivity. The five sublaminae of the IPL are indicated by the dotted lines. CAVIII-positive bipolar cell processes are evident in strata 3 of the IPL (horizontal arrow) and co-stratify with the middle band of calretinin staining. Scale bars: 10 μm. CAVIII, carbonic anhydrase-related protein VIII; GABA, γ-aminobutyric acid; INL, inner nuclear layer; IPL, inner plexiform layer. For interpretation of color references in figure legend, please refer to the Web version of this article.

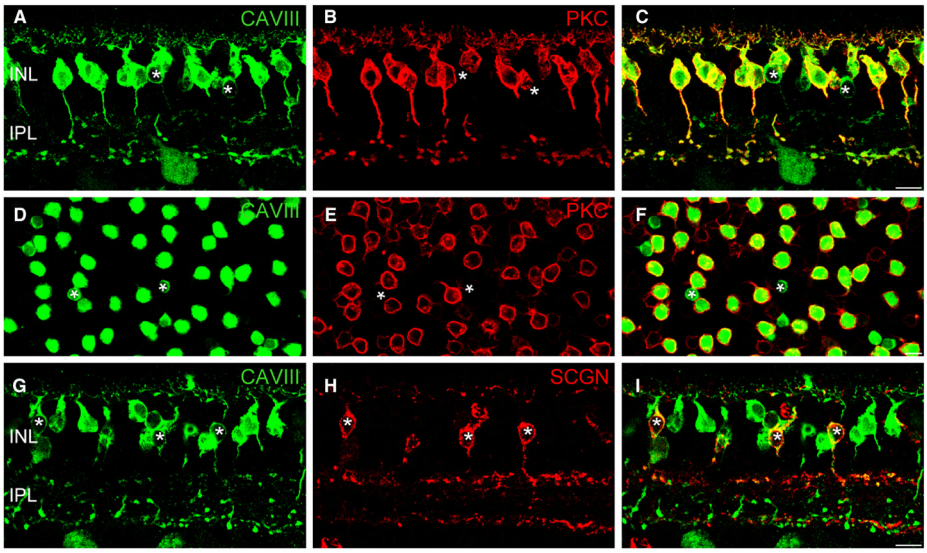

Fig. 4.

CAVIII is localized to RBCs and a subset of cone bipolar cells in the macaque retina. (A–F) Immunolocalization of CAVIII and PKC in vertical section (AC) and a whole-mount (D–F) of the macaque retina. The whole-mount image is taken with the focus at the levels of the distal INL. As in the mouse retina, most CAVIII-positive bipolar cells are also immunoreactive for PKC, indicating that they are RBCs (C and F). Asterisks indicate CAVIII-positive bipolar cells that lack PKC staining. (G–I) Vertical section labeled for CAVIII and SCGN shows CAVIII-positive bipolar cells that stratify in the outermost region of the IPL, indicating that CAVIII is present in DB1 OFF cone bipolar cells (asterisks). Scale bars: 10 μm. CAVIII, carbonic anhydrase-related protein VIII; INL, inner nuclear layer; IPL, inner plexiform layer; PKC, protein kinase C; SCGN, secretagogin.

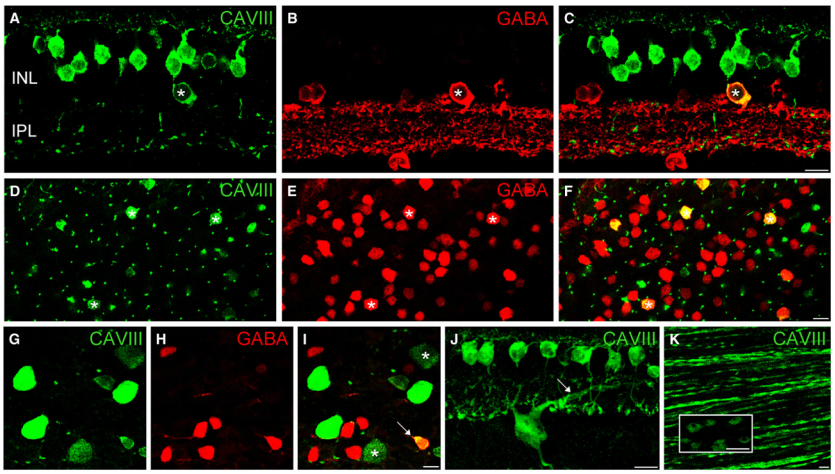

Fig. 5.

CAVIII is localized to a subset of GABAergic amacrine cells in the macaque retina. (A–I) Immunolocalization of CAVIII and GABA in a vertical section (A–C), a whole-mount at the level of the distal INL retina (D–F), and a whole-mount at the level of the GCL (G–I). Asterisks in A–F indicate CAVIII-positive amacrine cells that also contain GABA. The cell indicated by the arrowhead in (I) is an example of a CAVIII-positive displaced amacrine cell. Large (average diameter = 18 μm) CAVIII-positive ganglion cells were evident in the GCL. Approximately half of these showed strong CAVIII staining, whilst the other half showed relatively weaker CAVIII staining (asterisks). (J) Average confocal projection of a vertical section stained for CAVIII showing the stratification of one of the strongly stained ganglion cells. The main dendritic branch is targeted to the outer region of the IPL (arrow), indicating that it is an OFF-type ganglion cell. (K) Whole-mount focused at the level of the nerve fiber layer shows CAVIII immunoreactivity in ganglion cell axons. High-power inset shows that CAVIII is particularly abundant in bulbous varicosities on the axon. Scale bars: 10 μm. CAVIII, carbonic anhydrase-related protein VIII; GABA, γ-aminobutyric acid; INL, inner nuclear layer; IPL, inner plexiform layer.

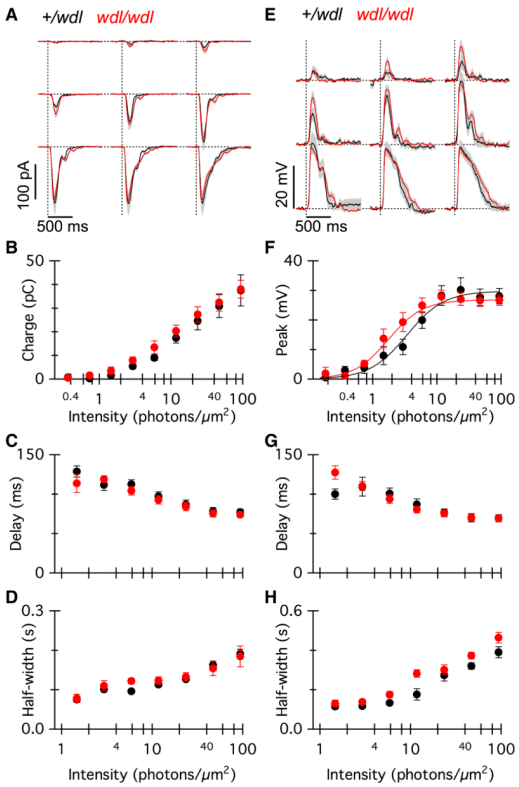

Fig. 6.

Light-evoked responses of RBCs are not altered in the *wdl* mutant. (A) Average flash-evoked EPSCs in RBCs from *wdl*/*wdl* (grey/red, $n = 12$) and *wdl*/+ littermates (black, $n = 8$). Individual flashes from each cell were averaged. The holding potential was −70 mV. Grey/red shading indicates ± 1 SEM. Flash strengths were 0.37, 0.73, 1.5, 2.9, 5.9, 11, 23, 47, 94 photons/μm^2. (B–D) Total charge transfer (B), delay to half-maximum amplitude (C) and response half-width (D) for the current responses in *wdl*/+ (black) and *wdl*/*wdl* (grey/red) mice as a function of flash strength. The two lowest flash intensities are not included in the quantitative data shown in (C) and (D), due to large variability in these parameters resulting from response failures. (E) Average flash-evoked EPSPs from the same group of cells as (A–D). (F–H) Peak voltage (F), delay to half-maximum amplitude (G) and response half-width (H) for the voltage responses in *wdl*/+ (black) and *wdl*/*wdl* (grey/red) mice as a function of flash strength. Similar to (C) and (D), the two lowest flash intensities are not included in the quantitative data shown in (G) and (H). Error bars indicate ± 1 SEM. For interpretation of color references in figure legend, please refer to the Web version of this article.

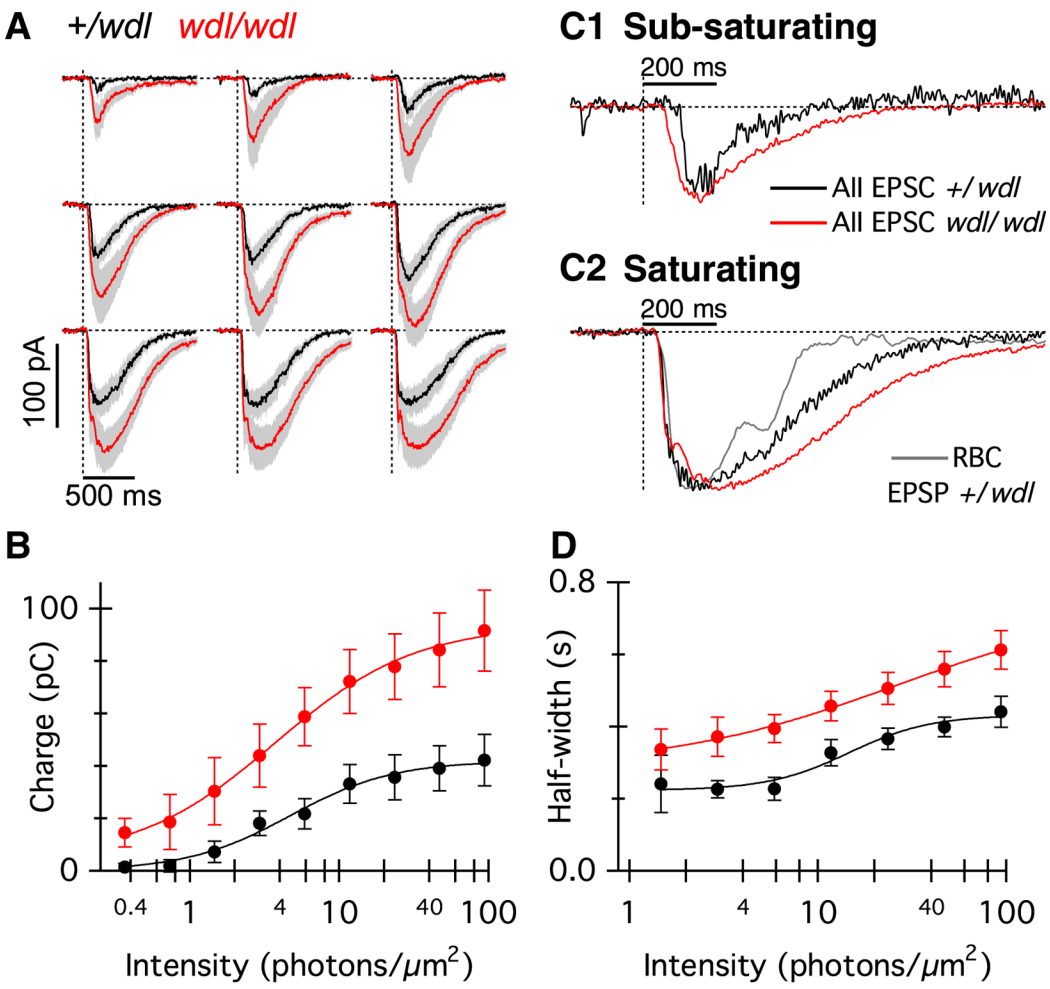

Fig. 7.

Light-evoked responses of AII-ACs are larger and more prolonged in *wdl* mutant mice. (A) Average flash-evoked EPSCs in AII-ACs from *wdl*/*wdl* (grey/red, $n = 10$) and *wdl*/+ littermates (black, $n = 10$). The holding potential was −70 mV. Grey/red shading indicates ± 1 SEM. Flash strengths were the same as those used in Fig. 6. (B) Total charge transfer for EPSCs in *wdl*/+ (black) and *wdl*/*wdl* mice (grey/red) plotted against flash intensity. (C1) Normalized average EPSCs from *wdl*/+ AII-ACs (black trace) and *wdl*/*wdl* AII-ACs (grey/red trace) to a light flash of sub-saturating intensity (1.5 photons/μm^2). (C2) The grey/red trace shows the normalized average EPSP from *wdl*/+ RBC, inverted for comparison with the AII-AC EPSCs. The normalized average AII-AC EPSCs are shown for *wdl*/+ (black) and *wdl*/*wdl* (grey/red). The flash intensity was close to saturating (47 photons/μm^2). Note that the AII-AC EPSCs are more prolonged than the RBC EPSP. The AII-AC EPSC in the *wdl*/*wdl* mutant is prolonged compared with the *wdl*/+ mice. (D) Response half-width in *wdl*/*wdl* mice (grey/red) and *wdl*/+ mice. Due to failures, and resulting large variability of the measurements, the two lowest flash intensities were excluded from the data shown in (D). EPSC, excitatory postsynaptic current; EPSP, excitatory postsynaptic potential; RBC, rod bipolar cell. For interpretation of color references in figure legend, please refer to the Web version of this article.

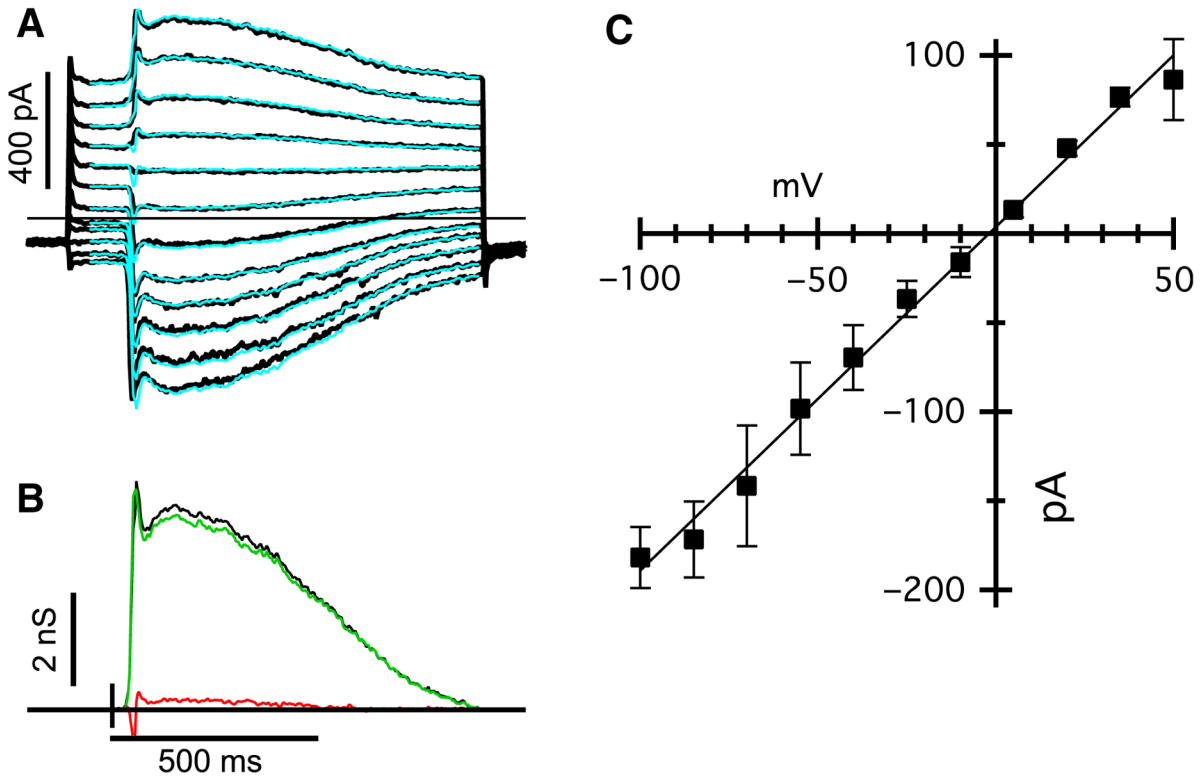

Fig. 8.

Light-evoked inputs to AII-ACs are linear in the *wdl* mutant mice. (A) Flash-evoked EPSCs in an AII-AC from a *wdl*/*wdl* animal. The holding potential was −70 mV. The superimposed cyan traces show the predicted currents reconstructed from the conductances shown below. (B) Excitatory (light grey/green) and inhibitory (dark grey/red) conductances required to account for the light-evoked currents shown above. The black shows the total conductance (excitation + inhibition) and indicates that the input can be accounted for almost entirely by excitation under these recording conditions. (C) Average current–voltage relation (± SEM) for four AII-ACs, including the one shown in (A) and (B). Before averaging, the individual current-voltage (IV) were normalized to the mean conductance for the data-set. The mean conductance was 2.0 ± 0.6 nS (n = 4). For interpretation of color references in figure legend, please refer to the Web version of this article.

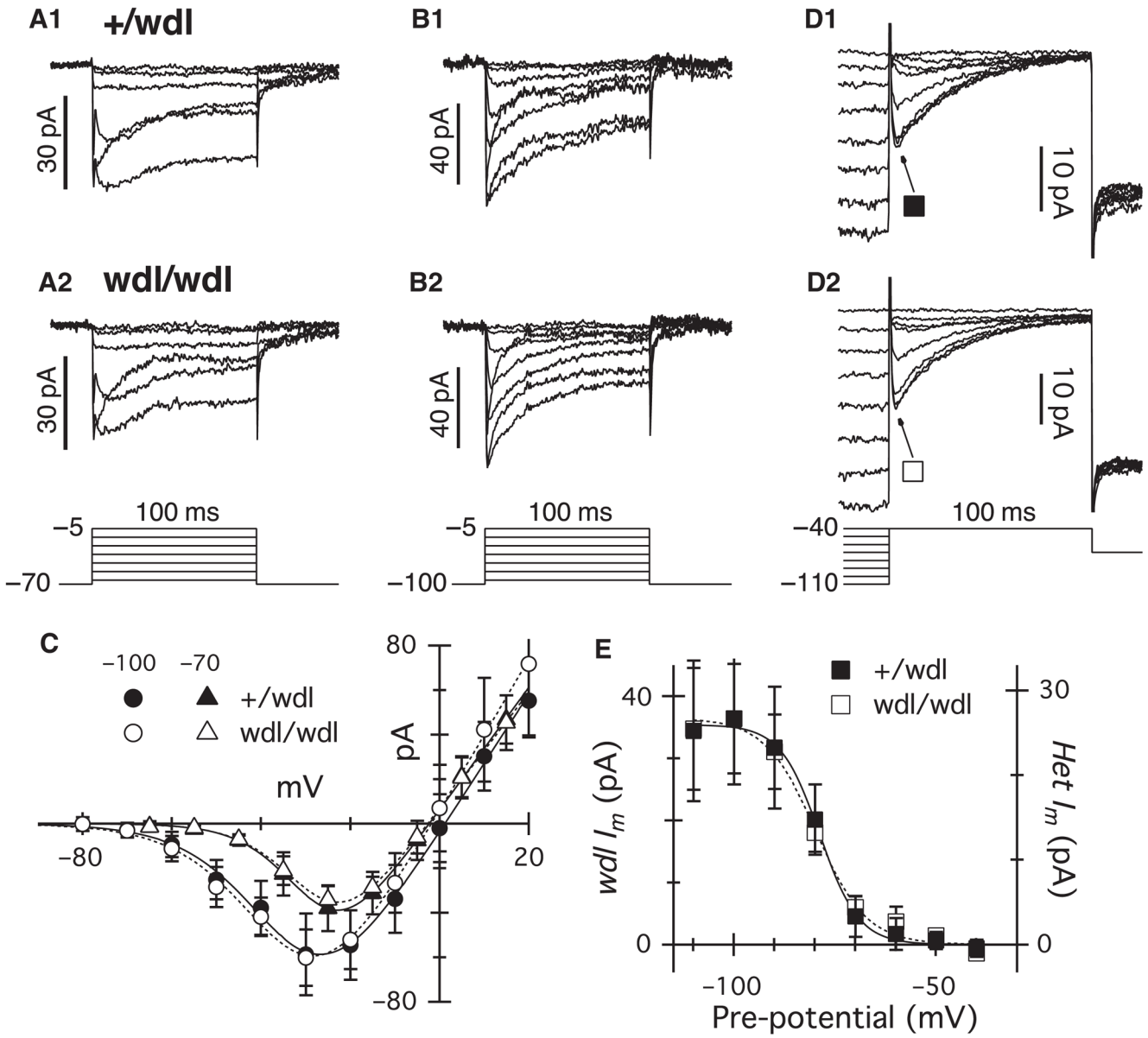

Fig. 9.

Calcium currents are indistinguishable in *wdl/wdl* and *wdl/+* mice. Leak subtracted currents recorded in RBCs from *wdl/+* (A1, $n = 11$; B1, $n = 8$; D1, $n = 7$) and *wdl/wdl* mice (A2, $n = 10$; B2, $n = 10$; D2, $n = 8$) during 100-ms depolarizing voltage pulses. The pipette solution contained $CsMeSO_4$ to block potassium currents. SR 95531 (10 μm), TPMPA (30 μm) and strychnine (1 μm) were added to the bath solution to block inhibitory currents. Depolarizing steps were applied in 10-mV increments from a holding potential of −70 mV (A) to activate mainly L-type calcium channels, or −100 mV (B) to activate both L- and T-type currents. (C) The amplitudes (± SEM) for average current–voltage relations from RBCs in the *+/wdl* (filled symbols) *and wdl/wdl* mouse (open symbols) were measured at a fixed time-point 10 ms after the onset of the voltage pulse. Triangles show currents measured from a holding potential of −70 mV, and circles show currents measured from a holding potential of −100 mV. (D) Steady-state inactivation of the transient component of the calcium current was generated by a 1-s pre-pulse to potentials between −110 and −40 mV. (E) The symbols show

the difference between the current measured 8 ms after the onset of the test pulse to −40 mV, and 90 ms later, at the end of the test pulse. Data from the +/*wdl* and mutant animals have been scaled for comparison. The smooth lines show a fit to a Boltzmann function, with half-inactivation potentials of −79 and −80 mV for the +/*wdl* and mutant data, respectively. The slope factors were 4.9 and 6.3 mV.

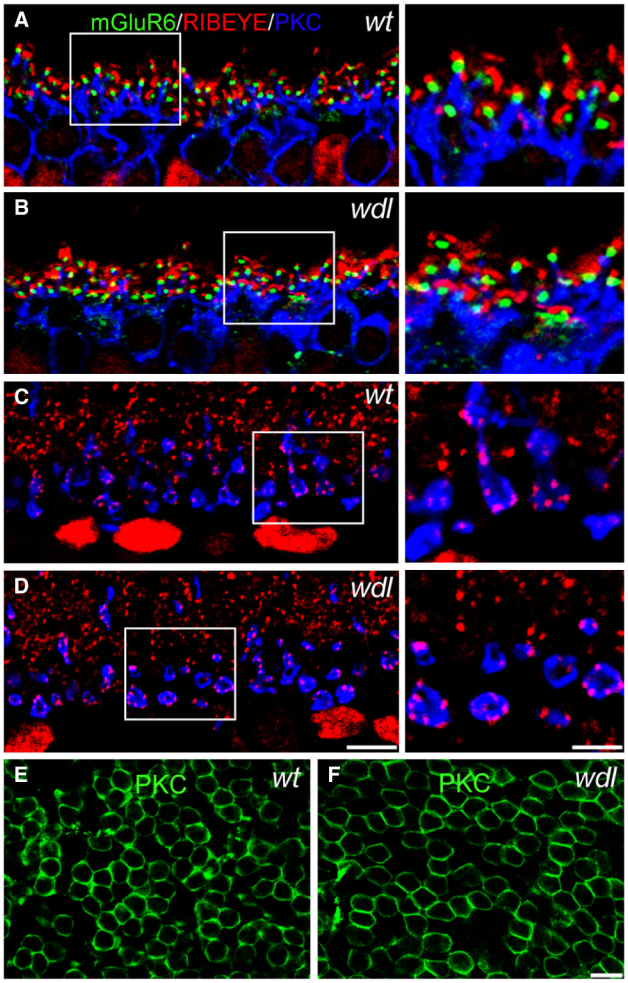

Fig. 10.

Normal ribbon synapses in the rod pathway of the *wdl* mutant mouse. (A–D) Vertical sections of the OPL from wild-type (WT) and mutant (*wdl*) retina labeled for mGluR6, RIBEYE and PKC. Right-hand panels show a magnified view of the region outlined by the dotted rectangles. (A and B) mGluR6 puncta can be seen at the tip of RBC dendrites adjacent to ribbon synapses in both the mutant and wt retina, indicating normal synaptic organization in the OPL. (C and D) RBC axon terminals show a similar density of RIBEYE positive ribbons in the wt and mutant retina. (E and F) Whole-mounts of *wt* and *wdl* retina stained for PKC and focused at the level of the INL. The density of PKC-positive RBC bodies is similar in the two retinas. Scale bars: 10 μm (A and B), (E and F); right-hand panels: 5 μm. PKC, protein kinase C.

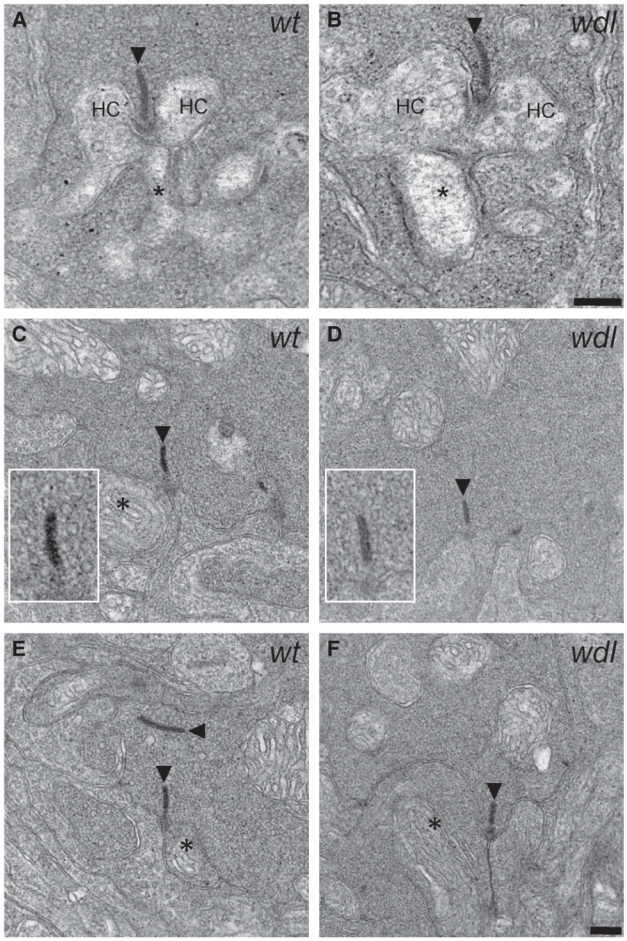

Fig. 11.

Normal ultrastructural organization of ribbon synapses in the rod pathway of the *wdl* mutant mouse. (A and B) Examples of rod spherules in a *wt* (A) and *wdl* mutant (B) mouse. In both cases, two horizontal cell (HC) processes and a central RBC dendrite make normal invaginations at the synaptic ribbon (arrowheads). (C and D) Examples of RBC axon terminals in the IPL of the *wt* (C, E) and *wdl* mutant (D, F). The overall appearance of the RBC axon terminal was similar in the two genotypes. In both cases, ribbons and mitochondria were evident, the terminals were filled with vesicles, and postsynaptic processes could be seen abutting the ribbon synapses. The insets show a 'halo' of docked vesicles surrounding the synaptic ribbon in both the *wt* and *wdl* mutant. Asterisks denote putative AII-AC processes. Scale bar: 200 nm.

Table 1

Primary antibodies used in this study

Antibody	Species	Dilution	Antigen	Source, catalog no.	Specificity
CAVIII	Rabbit	1: 50	Epitope corresponding to amino acids 1–100 mapping at the N-terminus of CAVIII of human origin	Santa-Cruz Biotechnology, Santa Cruz, CA #67330, USA	See Fig. 1
PKC	Mouse	1: 400	Amino acids 296–317 of PKC	Sigma, St Louis, MO #P5704, USA	Recognizes an 80-kDa polypeptide of PKC in bovine brain lysates
RIBEYE (Ctbp2)	Mouse	1: 2000	Amino acids 361–445 (C-terminus) of mouse CtBP2	BD Biosciences Pharmingen, San Diego, CA #612044, USA	Recognizes a 48-kDa band on Western blots of mouse brain smooth muscle-like cells (manufacturer's data sheet)
mGluR6	Guinea pig	1: 1000	Synthetic peptide corresponding to amino acids 853–871 of mouse mGluR6	Gift from Prof. Furukawa Takahisa, Osaka Bioscience Institute, Japan	Staining absent in mGluR6 knockout mouse (Koike *et al.*, 2010)
SCGN	Sheep	1: 2000–1: 5000	276 amino acids (full length) of recombinant human SCGN and 10 extra AA, N-terminal His-tag	Biovendor R&D (#RD184120100)	Pattern obtained with this antibody is identical to a non-commercial antibody that recognizes a 32-kDa band on Western blot of mouse retina and brain lysates (Puthussery *et al.*, 2010)
vGluT1	Guinea pig	1: 5000	Synthetic peptide (amino acids 542–560 of rat vGlut1)	Millipore #AB5905	Recognizes a 62-kDa band on Western blots of brain lysates (manufacturer's data sheet)
Calretinin	Goat	1: 1000	Rat calretinin	Millipore #AB1550	Detects a ~30-kDa band on Western blots of rat brain extracts (Winsky *et al.*, 1996)
GABA	Guinea pig	1: 5000	GABA coupled to KLH via glutaraldehyde	Millipore #AB175	Staining blocked by preadsorbing antibody with 100 μm GABA couples to glutaraldehyde (manufacturer's data sheet)

CAVIII, carbonic anhydrase-related protein VIII; GABA, γ-aminobutyric acid; PKC, protein kinase C; SCGN, secretagogin; vGluT1, vesicular glutamate transporter 1.